Quaternary Research (2022), 1–14
doi:10.1017/qua.2022.11

Research Article

Hydroclimatic changes in south-central China during the 4.2 ka event and their potential impacts on the development of Neolithic culture

Tianli Wang[a,b,c,†], Dong Li[d,†], Xing Cheng[e], Jianghu Lan[a], R. Lawrence Edwards[f,g], Hai Cheng[a,c], Xingxing Liu[a], Gang Xue[h], Hai Xu[i], Le Ma[a], Jingjie Zang[a], Yaqin Wang[j], Yongli Gao[k], Ashish Sinha[l] and Liangcheng Tan[a,c]*

[a]State Key Laboratory of Loess and Quaternary Geology, Institute of Earth Environment, Chinese Academy of Sciences, Xi'an 710061, China; [b]University of Chinese Academy of Sciences, Beijing 100049, China; [c]Institute of Global Environment Change, Xi'an Jiaotong University, Xi'an 710054, China; [d]Library of Chang'an University, Xi'an 710064, China; [e]Shaanxi Experimental Center of Geological Survey, Shaanxi Institute of Geological Survey, Xi'an 710054, China; [f]Department of Earth and Environmental Sciences, University of Minnesota, Minneapolis, Minnesota 55455, USA; [g]School of Geography, Nanjing Normal University, Nanjing 210097, China; [h]State Key Laboratory of Continental Dynamics, Department of Geology, Northwest University, Xi'an 710069, China; [i]Institute of Surface-Earth System Science, Tianjin University, Tianjin 300072, China; [j]Xi'an Institute for Innovative Earth Environment Research, Xi'an 710061, China; [k]Department of Geological Sciences, University of Texas at San Antonio, San Antonio, Texas 78249, USA and [l]Department of Earth Science, California State University, Carson, California 90747, USA

Abstract

The 4.2 ka event is widely presumed to be a globally widespread aridity event and has been linked to several episodes of societal changes across the globe. Whether this climate event impacted the cultural development in south-central China remains uncertain due to a lack of regional paleorainfall records. We present here stalagmite stable carbon isotope and trace element–based reconstruction of hydroclimatic conditions from south-central China. Our data reveal a sub–millennial scale (∼5.6 to 4.3 ka) drying trend in the region followed by a gradual transition to wetter conditions during the 4.2 ka event (4.3–3.9 ka). Together with the existing archaeological evidence, our data suggest that the drier climate before 4.3 ka may have promoted the Shijiahe culture, while the pluvial conditions during the 4.2 ka event may have adversely affected its settlements in low-lying areas. While military conflicts with the Wangwan III culture may have accelerated the collapse of Shijiahe culture, we suggest that the joint effects of climate and the region's topography also played important causal roles in its demise.

Keywords: Speleothem, Precipitation, Middle Yangtze River, Shijiahe culture, Late Holocene, 4.2 ka event

(Received 24 November 2021; accepted 3 March 2022)

INTRODUCTION

The role of abrupt climatic change in shaping cultural evolution and social development during the Holocene is a focal topic in paleoclimate research (Sinha et al., 2019; Dong et al., 2021; Tan et al., 2021). The nearly global cooling/drought anomaly between 4.2 and 3.9 ka, known as the 4.2 ka event, has been used to define a new stratigraphic stage, the Meghalayan Age (Bond et al., 1997; Berkelhammer et al., 2012; Railsback et al., 2018). Since Weiss et al. (1993) first identified the link between the 4.2 ka event and the collapse of the Akkadian Empire, several studies have also attributed the demise of civilizations such as ancient Egypt (Weiss and Bradley, 2001), Mesopotamia (deMenocal, 2001; Watanabe et al., 2019), the Indus valley civilization (Staubwasser et al., 2003; Berkelhammer et al., 2012), and Neolithic cultures in China (Wu and Liu, 2004; Yang et al., 2015; Xiao et al., 2018; Cai et al., 2021) to the 4.2 ka event.

The Shijiahe culture based in the middle Yangtze River basin in south-central China was a socially complex Neolithic culture with a state-like civilization system (Han, 2016). Archaeological data suggest that it declined sometime between 4.1 and 3.9 ka (State Administration of Cultural Heritage of China, 2002; Zhong, 2019; Han, 2020b). Although the fall of Shijiahe culture is widely attributed to its military defeat by the Wangwan III culture (H. Wang, 2013; Han, 2020a, 2020b), two pertinent questions remain: (1) The Shijiahe culture was stronger than Wangwan III culture, as evidenced by its large-scale sites, complicated sociopolitical structure, and solid defense system (Han, 2020b), so why did it lose to a relatively weaker state? (2) The archaeological excavations suggest that the Shijiahe sites featured advanced city walls and courtyard buildings (State Administration of Cultural Heritage of China, 2002), which were unique during the Neolithic period, so why did the post-Shijiahe culture not occupy these sites, instead inhabiting new sites at higher elevation (Zhong, 2019)?

Although the timing of the Shijiahe culture's demise coincides with cultural collapses in other regions, whether climatic change contributed to its downfall requires further investigation. The

*Corresponding author at: State Key Laboratory of Loess and Quaternary Geology, Institute of Earth Environment, Chinese Academy of Sciences, Xi'an 710061, China. E-mail address: tanlch@ieecas.cn (L. Tan).

†Joint first authors: T. Wang and D. Li.

Cite this article: Wang T *et al* (2022). Hydroclimatic changes in south-central China during the 4.2 ka event and their potential impacts on the development of Neolithic culture. *Quaternary Research* 1–14. https://doi.org/10.1017/qua.2022.11

Holocene climatic records of the East Asian summer monsoon (EASM) indicate that the 4.2 ka event was characterized by a weaker monsoon in China with less monsoonal moisture reaching northern China (Wang et al., 2005; Tan et al., 2018a). The climatic conditions in central and southern China during the time are, however, debated. For example, by comparing hydrological records from China, Tan et al. (2018a) proposed a view of "wet in central and southern China and arid in northern China" during this period. Similarly, Zhang et al. (2018) considered the northern Qinling Mountain–lower Yangtze River region to be the dry–wet boundary and suggested that south-central China experienced a humid period during the 4.2 ka event. Wu and Liu (2004) also demonstrated that frequent floods marked the 4.2 ka event in south-central China. In contrast, Sun et al. (2019) and Liu and Feng (2012) concluded cold-dry conditions in central and southern China during the period. The sedimentary pollen and geochemical records from the Sanfangwan (Jia et al., 2017) and Tanjialing sites (Li et al., 2013) also indicate an arid period in the Jianghan Plain in south-central China during the 4.2 ka event, even though flood events were also reported in these records.

These discrepancies among studies stem largely from a lack of precisely dated paleorainfall records from south-central China. Although several speleothem records are available from central and southern China, for example, from the Sanbao (Dong et al., 2010; Cheng et al., 2016a), Lianhua (LH) (Cosford et al., 2008; H. Zhang et al., 2013), and Dongge (DG) Caves (Yuan et al., 2004; Wang et al., 2005), the climatic significance of these stalagmite $\delta^{18}O$ records is highly debated and subject to multiple interpretations (e.g., moisture sources and pathways, upstream rainout, and regional rainfall) (Yuan et al., 2004; Maher and Thompson, 2012; Tan et al., 2018a). The $\delta^{13}C$ and trace elements ratios (e.g., Sr/Ca, Mg/Ca, and Ba/Ca) in stalagmites, which reflect the local hydrological environment (Fairchild and Treble, 2009; Xue et al., 2021; Zhang et al., 2021), are thus better suited to reconstruct the local rainfall variability. In this study, we present a suite of stalagmite-based stable isotope ($\delta^{18}O$, $\delta^{13}C$) and trace element records (Sr/Ca, Mg/Ca, Ba/Ca) from Remi Cave, Hunan Province, aiming to reconstruct the monsoon precipitation variations in south-central China across the 4.2 ka event. Our data, together with the archaeological evidence from the region, can help to clarify the possible links between the demise of Shijiahe culture and climatic change.

STUDY AREA AND MATERIAL

Remi Cave (RM, also called Wulong Cave, 29°13′36″N, 109°21′28″E, elevation 872.5 m) is situated in Longshan County of Hunan Province in the middle Yangtze River (Fig. 1A). The cave formed in Paleozoic carbonates in the Wulong Mountains. The study area has a subtropical humid monsoon climate. Meteorological data (1981–2010 CE) from Longshan station indicate the region is strongly affected by the EASM, with average annual air temperature and total precipitation of 16.1°C and ∼1300 mm, respectively (Fig. 1B). The summer season rainfall contributes to more than 70% of annual rainfall at the site from April to September (Fig. 1B).

The cave is ∼10 km long and contains two chambers, with the front chamber open to the public. A large number of stalagmites and stalactites are found ∼200 m away from the cave entrance, with many stalagmites reaching heights above 5 m or even 10 m. A columnar-shaped aragonite stalagmite RM8, ∼17 cm in length and 10–12 cm in diameter, was collected from the front chamber in 2016. After splitting and polishing, two potential hiatuses were observed at 4 cm and 10 cm depths, respectively (Fig. 2A). Here, we focus on the bottom part (RM8-2, below the second hiatus) of the stalagmite, as its growth time covers the 4.2 ka event.

METHODS

A total of 19 subsamples for ^{230}Th dating were drilled parallel to the growth planes of RM8-2, each weighing 30–40 mg. The chemical procedures used to separate Th and U followed those described by Edwards et al. (1987). The measurements were made on a multicollector inductively coupled mass spectrometer at the University of Minnesota, USA (13 measurements), and the Institute of Global Environment Change Xi'an Jiaotong University (6 measurements), following the procedure described by Cheng et al. (2013).

Subsamples for stable isotope ($\delta^{18}O$, $\delta^{13}C$) analyses were drilled along the central growth axis of RM8-2 at average intervals of 0.5 mm. A total of 91 subsamples were measured using an IsoPrime100 gas source stable isotope ratio mass spectrometer equipped with a MultiPrep system at the Speleological Laboratory at the Institute of Earth Environment, Chinese Academy of Sciences (IEECAS). Samples of the Chinese standard TB1 were analyzed every 10–15 subsamples to check data reproducibility. Measurement precisions was <0.1‰ for $\delta^{18}O$ and $<$ 0.08‰ for $\delta^{13}C$ with 2σ analytical errors. All stable isotope compositions are reported in per mil relative to Vienna Pee Dee Belemnite.

Ninety-one subsamples (each ∼1 mg in weight) were also drilled for trace elements (Sr/Ca, Mg/Ca, Ba/Ca) analyses. The powders were dissolved in 2–4 mL 5% HNO_3 before being measured on an Agilent 5110 Inductively Coupled Plasma Optical Emission Spectrometer (ICP-OES) at the Speleological Laboratory at IEECAS. One in-house standard, W2, was measured every 5 subsamples, and the precision of X/Ca is <1% (X refers to Sr, Mg, and Ba). In addition, highly resolved Sr and Ca counts were analyzed using the fourth-generation Avaatech X-ray fluorescence (XRF) core scanner at IEECAS with a scan resolution of 0.1 mm. The details of this noninvasive method were reported in Li et al. (2019b).

RESULTS

The ^{230}Th dating results are listed in Table 1 and Figure 2B and C. The age of the RM8-6a subsample is not accurate, having a high $^{230}Th/^{232}Th$ ratio (Table 1), so this subsample was excluded from the study. The remaining 18 dates are all in stratigraphic order with dating uncertainties less than 0.2%. We established the chronological models of RM8-2 by linear interpolation and COPRA (Breitenbach et al., 2012), respectively (Fig. 2B and C). To facilitate comparisons with previous records (e.g., from LH, DG, and Heshang [HS] Caves), the age model based on linear interpolation was used in this study. The results show that RM8-2 grew between 5.667 and 3.885 ka (Fig. 2B). The growth rate of RM8-2 is also displayed in Fig. 2D.

The stable isotope records have a temporal resolution higher than 15 years. RM8-2 $\delta^{18}O$ values range from −6.74‰ to −4.73‰ and are relatively stable during 5.1–3.9 ka (Fig. 3A–C). The overall $\delta^{18}O$ trend is broadly replicated in DG (Dykoski et al., 2005) and LH (H. Zhang et al., 2013) cave records (Fig. 3A and B), suggesting the near-isotopic equilibrium

https://doi.org/10.1017/qua.2022.11 Published online by Cambridge University Press

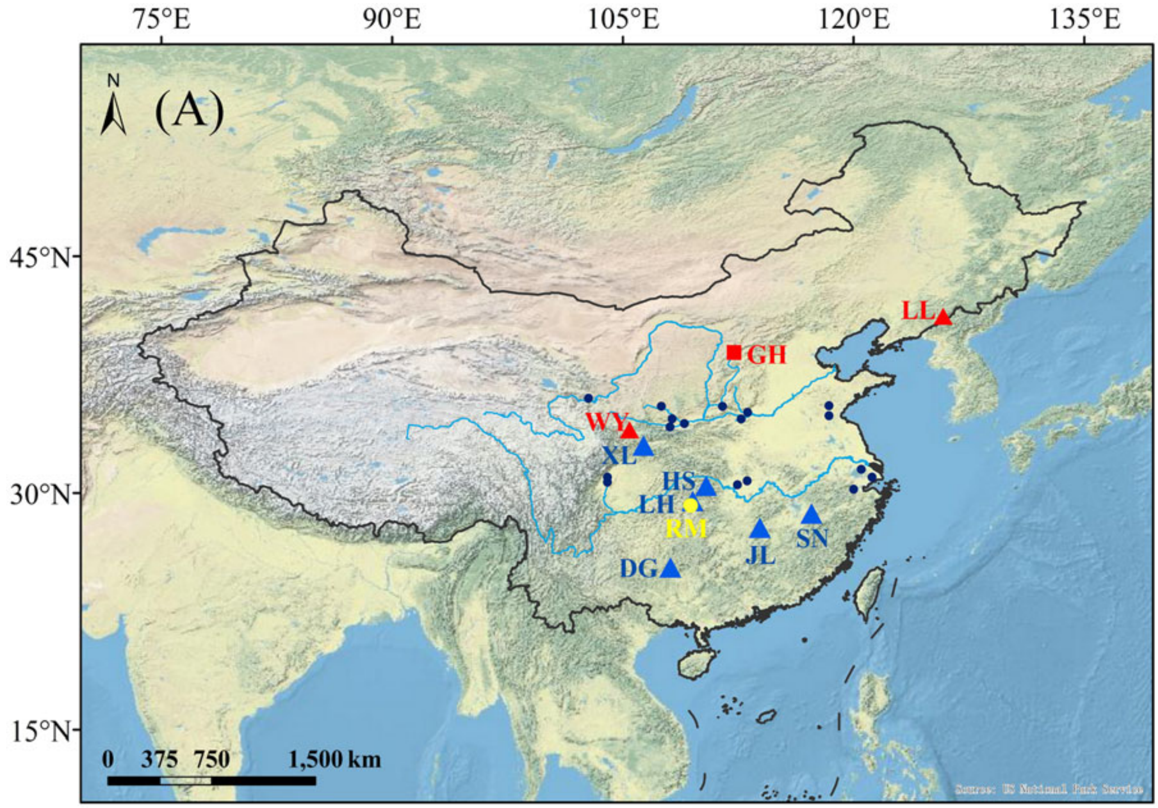

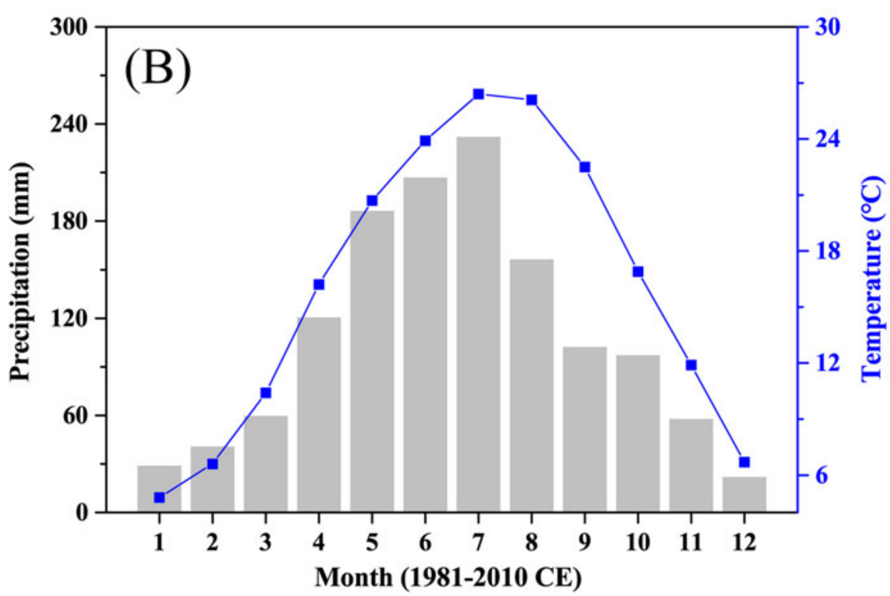

Figure 1. (A) Locations of Remi Cave (yellow circle) and other caves (triangles) and a lake (square) mentioned in this study: Lianhua (LH), Heshang (HS), Dongge (DG), Jiulong (JL), Shennong (SN), Xianglong (XL), Wuya (WY), Liuli (LL) Caves, and Gonghai (GH) Lake. The different colors reflect the wet (blue) and dry (red) conditions in China, respectively. The records of catastrophic floods during the 4.2 ka event are marked by small deep-blue dots. (B) Climatic setting of the study region with meteorological records from Longshan station. The gray bars and blue squares separately represent regional monthly average precipitation and mean air temperature during 1981–2010 CE.

deposition of RM8-2 according to the replication test (Dorale and Liu, 2009). RM8-2 $\delta^{13}C$ values vary between −4.46‰ and −2.36‰. A gradually increasing trend is observed between ~5.475 and 4.307 ka. Afterward, the $\delta^{13}C$ values exhibit a decreasing trend, superimposed with sharply fluctuating values, with two of the more depleted excursions at 4.207 and 3.925 ka (Fig. 3D).

X/Ca values of RM8-2 range from 0.254 to 0.393 mmol/mol for Sr/Ca, from 0.111 to 0.195 mmol/mol for Mg/Ca, and from 0.052 to 0.072 mmol/mol for Ba/Ca (Fig. 3E–G). XRF-based Sr/Ca varies from 2.70×10^{-3} to 4.17×10^{-3}, with an average value of 3.32×10^{-3}. The mean temporal resolution is ~3.73 years. As illustrated in Figure 3E, the Sr/Ca ratios obtained by the two methods (XRF and ICP-OES) show similar trends, indicating

https://doi.org/10.1017/qua.2022.11 Published online by Cambridge University Press

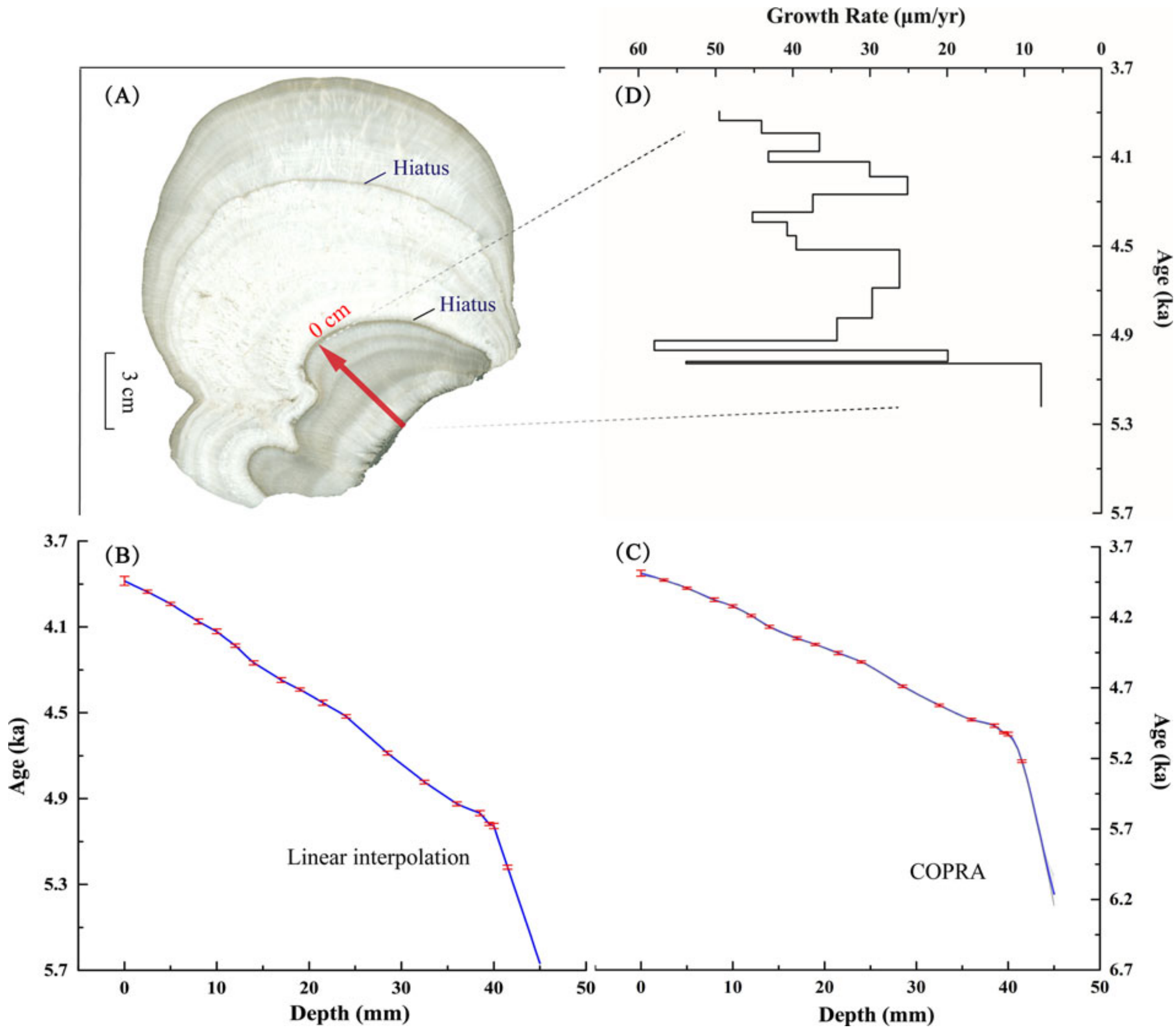

Figure 2. (A) Polished section of stalagmite RM8 with two obvious hiatuses. The red arrow in A denotes the growth axis of RM8-2, whose age model is shown using a linear interpolation method (B) and as established by COPRA (C). The depth (0 mm) of the two models begins from the second hiatus. The age model based on linear interpolation (B) was used in this study. (D) The growth rate of RM8-2.

the reliability of the high-resolution XRF scanning method (Li et al., 2019b).

DISCUSSION

Interpretation of proxies

The climatic significance of $\delta^{18}O$ of Chinese stalagmites has been intensely debated in recent years (Cheng et al., 2019). The climatic interpretation of stalagmite $\delta^{18}O$ in south-central China is particularly complex, and several mechanisms have been suggested as exerting influence on the $\delta^{18}O$ of precipitation and stalagmites, including moisture sources and pathways (Maher and Thompson, 2012; Li et al., 2019a), upstream rainout (Yuan et al., 2004; Hu et al., 2008), and regional and local rainfall amounts (Tan et al., 2018a). Given these complexities, we have mainly used the RM8-2 $\delta^{13}C$ and X/Ca in this study to reconstruct the local hydroclimate.

The $\delta^{13}C$ values in speleothems can vary with soil CO_2 concentrations and the dissolution of bedrock (Genty et al., 2001). Their contributions to speleothem $\delta^{13}C$ are further influenced by vegetation types and density above the cave, as well as the hydrological process in the cave system, for example, water–rock interaction (WRI) and prior aragonite or calcite precipitation (PAP/PCP) (Genty et al., 2003; McDermott, 2004; Tan et al., 2020b). The significant negative correlations of $\delta^{13}C$ with X/Ca ($r = -0.239$, $P < 0.05$ for Mg/Ca; $r = -0.362$, $P < 0.01$ for Sr/Ca; $r = -0.343$, $P < 0.01$ for Ba/Ca; $N = 91$; Fig. 4) exclude PAP/PCP processes as primary drivers of the $\delta^{13}C$ variations (Novello et al., 2019). It is therefore likely that the RM8-2 $\delta^{13}C$ variations were dominated by changes in vegetation coverage and biomass density above the cave, consistent with the explanations of speleothem $\delta^{13}C$ from LH (Cosford et al., 2009), which showed a variation trend similar to our records, despite differences in minor details (Fig. 5A). Those variations were further related to regional climatic conditions (e.g., temperature and precipitation changes) as demonstrated by modern investigations (Huang et al., 2013; Liu and Qu, 2019). In this process, rainfall amount plays an essential role. It was found that the net primary productivity of vegetation in south-central China continually declined due to decreasing

Table 1. U-Th isotopic compositions and ^{230}Th ages of RM8-2.[a]

Depth mm	Sample no.	^{238}U (ppb)		^{232}Th (ppt)		^{230}Th / ^{232}Th (atomic × 10^{-6})		δ^{234}U[b] (measured)		^{230}Th / ^{238}U (activity)		^{230}Th age (yr) (uncorrected)		^{230}Th age (yr) (corrected)		$\delta^{234}U^{c}_{initial}$ (corrected)		^{230}Th age (yr)[d] (corrected)	
0.5	RM8-1a	6454.5	±10.8	19,633	±394	653	±13	2338.0	±3.7	0.1204	±0.0003	3990	±10	3964	±21	2364	±4	3896	±21
2.5	RM8-2a	3308.0	±3.3	643	±14	10,274	±217	2346.2	±2.5	0.1212	±0.0002	4006	±7	4004	±8	2373	±3	3936	±8
5	RM8-3a	3768.7	±4.0	326	±7	23,486	±527	2358.7	±2.7	0.1233	±0.0002	4061	±7	4061	±8	2386	±3	3993	±8
8	RM8-4a	5152.0	±5.2	8179	±164	1296	±26	2324.1	±2.4	0.1248	±0.0002	4157	±7	4143	±12	2351	±2	4075	±12
10	RM8-1b	4349.5	±8.2	1541	±31	5836	±118	2309.9	±3.5	0.1254	±0.0003	4195	±11	4192	±11	2337	±4	4121	±11
12	RM8-5a	3616.1	±4.2	708	±15	10,694	±220	2304.5	±2.6	0.1271	±0.0002	4257	±8	4256	±8	2332	±3	4188	±8
14	RM8-2b	4294.2	±7.2	1185	±24	7783	±158	2324.1	±3.1	0.1303	±0.0003	4341	±10	4338	±10	2353	±3	4267	±10
15.5[e]	RM8-6a	5355.1	±6.3	20	±3	597,693	±84980	2310.7	±2.4	0.1333	±0.0002	4462	±8	4461	±8	2340	±2	4393	±8
17	RM8-3b	4187.1	±7.3	1560	±32	5832	±118	2302.5	±3.3	0.1318	±0.0003	4422	±11	4419	±11	2331	±3	4348	±11
19	RM8-7a	5021.6	±5.0	1197	±24	9237	±187	2315.8	±2.3	0.1335	±0.0002	4462	±7	4460	±7	2345	±2	4392	±7
21.5	RM8-4b	3656.0	±4.8	3854	±77	2100	±42	2282.8	±2.6	0.1343	±0.0003	4533	±10	4524	±12	2312	±3	4453	±12
24	RM8-8a	4888.3	±4.5	1436	±29	7565	±153	2257.1	±2.2	0.1348	±0.0002	4587	±8	4584	±8	2286	±2	4516	±8
28.5	RM8-9a	6576.2	±6.7	4094	±82	3670	±74	2227.7	±2.4	0.1386	±0.0002	4762	±8	4756	±9	2258	±2	4688	±9
32.5	RM8-10a	4418.2	±4.8	315	±7	33,552	±757	2289.9	±2.7	0.1450	±0.0002	4892	±8	4891	±8	2322	±3	4823	±8
36	RM8-11a	4973.0	±4.9	1955	±39	6165	±124	2266.7	±2.3	0.1470	±0.0002	4997	±9	4993	±9	2299	±2	4925	±9
38.5	RM8-1c	4844.7	±8.5	521	±11	22,815	±481	2279.8	±3.2	0.1489	±0.0003	5040	±12	5039	±12	2312	±3	4968	±12
39.5	RM8-12a	5239.5	±5.0	556	±12	23,312	±490	2278.1	±2.0	0.1502	±0.0002	5087	±7	5086	±7	2311	±2	5018	±7
40	RM8-5b	4952.9	±8.3	633	±13	19,404	±405	2277.4	±3.0	0.1505	±0.0003	5100	±13	5099	±13	2310	±3	5028	±13
41.5	RM8-13a	5142.1	±5.8	733	±16	18,412	±393	2344.2	±2.6	0.1592	±0.0002	5289	±9	5288	±9	2379	±3	5220	±9

[a]Analytical errors are 2σ of the mean. U decay constants: $\lambda_{238} = 1.55125 \times 10^{-10}$, $\lambda_{234} = 2.82206 \times 10^{-6}$. Th decay constant: $\lambda_{230} = 9.1705 \times 10^{-6}$. Corrected ^{230}Th ages assume the initial ^{230}Th/^{232}Th atomic ratio of $4.4 \pm 2.2 \times 10^{-6}$. Those are the values for a material at secular equilibrium, with the bulk earth ^{232}Th/^{238}U value of 3.8. The errors are arbitrarily assumed to be 50%.

[b]$\delta^{234}U = ([^{234}U/^{238}U]_{activity} - 1) \times 1000$.

[c]$\delta^{234}U_{initial}$ was calculated based on ^{230}Th age (T), i.e., $\delta^{234}U_{initial} = \delta^{234}U_{measured} \times e^{\lambda 234 \times T}$.

[d]Ages before 1950 CE.

[e]RM8-6a (in red) data are excluded from this study.

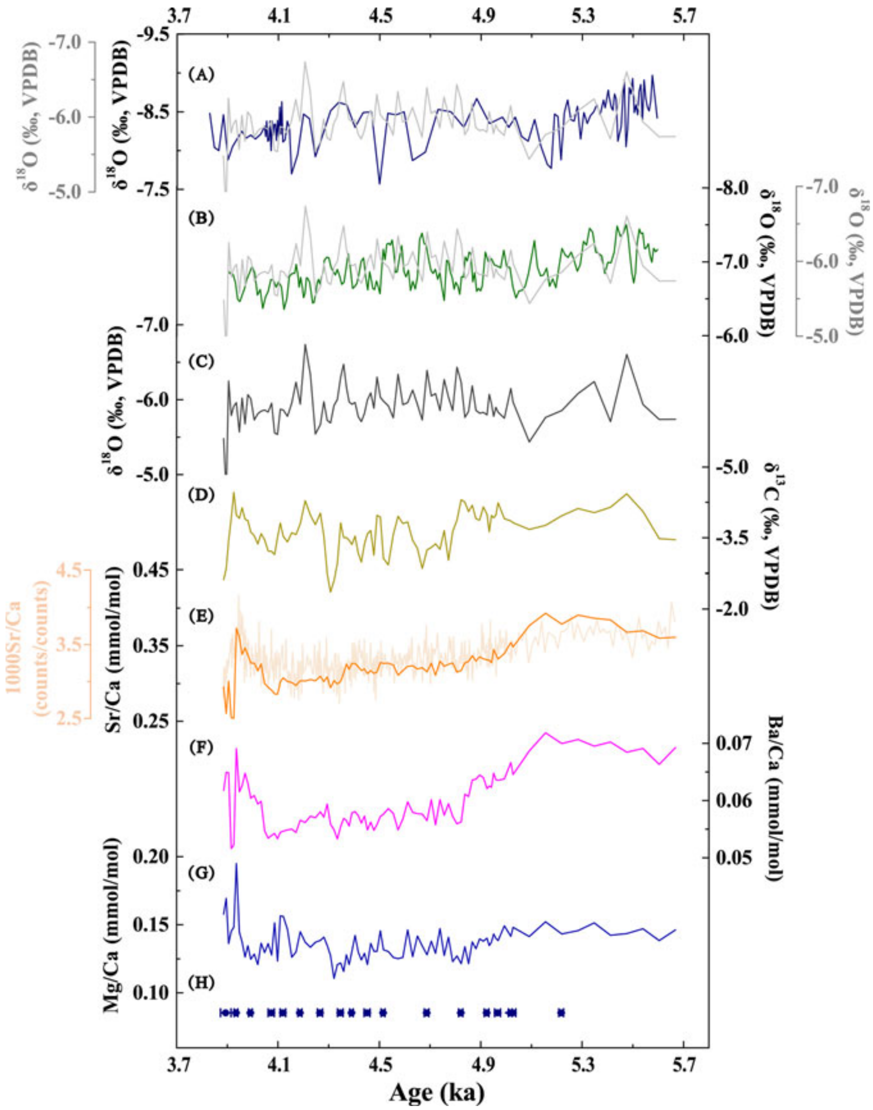

Figure 3. Stable isotopes and X/Ca records of RM8-2. (A, gray), (B, gray) and (C) all show the δ^{18}O sequence of RM8-2, whose overall variation pattern is parallel with stalagmite δ^{18}O records from Dongge Cave (A, dark blue) (Dykoski et al., 2005) and Lianhua Cave (B, green) (Zhang et al., 2013). The remaining records are δ^{13}C (D), X-ray fluorescence (XRF)-scanned (E, light orange), and optical emission spectrometry–based Sr/Ca (E, dark orange), Ba/Ca (F), and Mg/Ca (G) of RM8-2. (H) Dating errors of RM8-2.

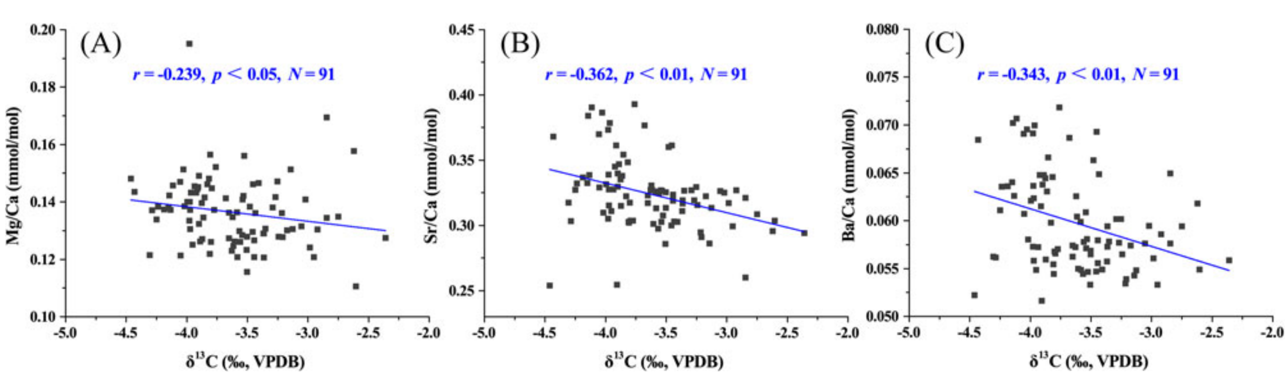

Figure 4. Cross-correlations between δ^{13}C and X/Ca of RM8-2. (A) δ^{13}C vs. Mg/Ca; (B) δ^{13}C vs. Sr/Ca; (C) δ^{13}C vs. Ba/Ca. Significant negative correlations occur between δ^{13}C and the X/Ca of RM8-2.

https://doi.org/10.1017/qua.2022.11 Published online by Cambridge University Press

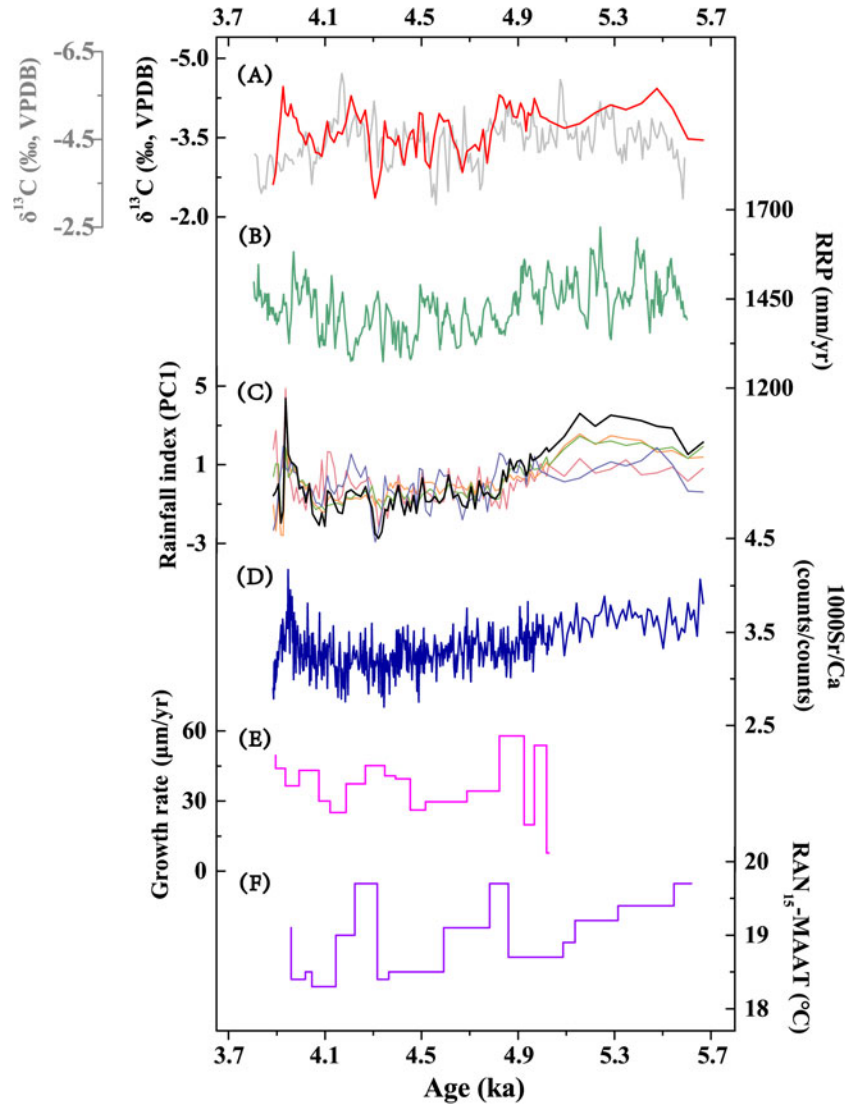

Figure 5. Comparation of RM8-2 records with other climate reconstructions. (A) RM8-2 $\delta^{13}C$ in red, and Lianhua (LH) $\delta^{13}C$ in gray. (B) Reconstructed regional precipitation (RRP), which is obtained by differencing coeval $\delta^{18}O$ values of Heshang (HS) and Dongge (DG) Caves (Hu et al., 2008). (C) PC1 (black) of RM8-2 $\delta^{13}C$ (purple), Mg/Ca (red), Sr/Ca (orange), and Ba/Ca (green) records as regional rainfall index. (D) X-ray fluorescence (XRF)-scanned Sr/Ca of RM8-2. (E) The growth rate of RM8-2. (F) RAN_{15}-MAAT (mean annual air temperature) record, which is reconstructed from stalagmite HS4 and represents regional temperature change (Wang et al., 2018).

rainfall during 2009–2012 CE (Huang et al., 2013). On the other hand, the carbon cycle research in the underground river of the Dalong Cave (~150 km away from RM Cave) shows $\delta^{13}C$ was negatively correlated with rainfall amount (Wang, 2013b). Under wet conditions, dense overlying vegetation produces more soil CO_2 by enhancing plant roots' respiration and increasing soil bioproductivity, resulting in lighter speleothem $\delta^{13}C$ values (McDermott, 2004; Fohlmeister et al., 2011). Although the HCO_3^- concentration in seepage would increase and corrode more bedrock, its positive effects on $\delta^{13}C$ values seem to be overridden by the soil CO_2-derived negative effects (W. Wang, 2013). For these same reasons, RM8-2 $\delta^{13}C$ variations could reflect regional precipitation, with lower values indicating enhanced precipitation. Indeed, the RM8-2 $\delta^{13}C$ profile varies inversely with the reconstructed regional precipitation, which was obtained by differencing coeval $\delta^{18}O$ values of the HS and DG Caves (Hu et al., 2008; Fig. 5B).

Factors influencing X/Ca ratios in speleothems are diverse, including hydrological processes (e.g., WRI, PAP/PCP), temperature, and speleothem growth rate, among others (Treble et al., 2003; Fairchild and Treble, 2009; Tan et al., 2014; Xue et al., 2021). In previous studies, trace elements varying positively in tandem with $\delta^{13}C$ were suggested to be caused by rainfall-related hydrological processes (Cheng et al., 2016b; Tan et al., 2020b; Xue et al., 2021). Specifically, under dry climate conditions, prolonged WRI could increase the dissolution of bedrock. At the same time, low CO_2 pressure in overlying soil due to sparse vegetation cover promotes CO_2 degassing and PCP. These two processes jointly push speleothem X/Ca and $\delta^{13}C$ toward higher values (Fairchild et al., 2000; Fairchild and Treble, 2009). Another issue is that Mg/Ca positively correlates with $\delta^{13}C$, but Sr/Ca shows an inverse variation when PAP rather than PCP occurred before stalagmite deposition (Fairchild and Treble, 2009; Wassenburg et al., 2016; Ronay et al., 2019). However, in this study, X/Ca ratios vary in

https://doi.org/10.1017/qua.2022.11 Published online by Cambridge University Press

the same direction, and their variation trends are in contrast to $\delta^{13}C$, which cannot be explained by either of these two mechanisms. These unusual variations may be related to the enhanced (weakened) WRI efficiency under wet (dry) hydrological conditions, because the higher (lower) HCO_3^- concentration in seepage due to increasing (decreasing) plant coverage and biomass under wet (dry) conditions would dissolve more (less) bedrock per unit time and carry more (less) trace elements into stalagmites. Meanwhile, when carbonate is oversaturated due to the ongoing and relatively rapid dissolution of bedrock, PCP would also occur, resulting in increased X/Ca in stalagmites. The investigation in the Dalongdong underground river confirms the critical roles of soil CO_2 and rainfall amount on the X/Ca variations in underground water (W. Wang, 2013). In addition, more trace elements in the overlying soil would be washed into stalagmites by heavy rainfalls. Given this, we suggest the X/Ca variations of RM8-2 could also reflect local hydrological conditions, with higher ratios reflecting increasing rainfall and therefore intensified vegetation coverage. The influence of temperature and growth rate on RM8-2 X/Ca seems minor, as they cannot make X/Ca variations so similar (Huang et al., 2001; Fairchild and Treble, 2009; Fig. 5). The growth rate of RM8-2 varied in parallel with X/Ca because it may also be controlled by rainfall amount (Fig. 5), with higher rates occurring when rainfall increased.

Given the X/Ca and $\delta^{13}C$ variations of RM8-2 all reflect local rainfall conditions, principal component analysis (PCA) was used to extract their common variations. It should be noted that inverse $\delta^{13}C$ values were used during the process, as $\delta^{13}C$ shows an inverse relationship with X/Ca. PC1 explains 57% of the variation and can be regarded as a rainfall index (Fig. 5C).

Hydroclimate in south-central China and regional comparison covering the 4.2 ka event

The rainfall index and Sr/Ca of RM8-2 decreased gradually from 5.6 to 4.3 ka, indicating a drying trend (Fig. 6). After that, their variation trends reversed at 4.3–4.2 ka, implying gradually wetter conditions during ∼4.3–3.9 ka, which corresponds to the 4.2 ka event (Railsback et al., 2018). The inferred wet conditions over south-central China are supported by the reconstructed regional precipitation between HS and DG Caves (Hu et al., 2008) and the climatic conditions revealed by the Shennong (SN) $\delta^{13}C$ profile (Zhang et al., 2021; Fig. 6). This is also consistent with the speleothem-based studies in Jiulong (JL) (Zhang et al., 2021) and Xianglong (XL) Caves and may explain the faster growth rate of the stalagmite in the LH Cave during this period (H. Zhang et al., 2013), in contrast with the pronounced dry conditions that were widely reported in northern China during the time (Chen et al., 2015; Yang et al., 2015; Xiao et al., 2018). For example, the pollen-based precipitation records at Gonghai Lake (Chen et al., 2015) and speleothem $\delta^{13}C$ from Liuli (LL) (Zhao et al., 2021) and Wuya (WY) Caves (Tan et al., 2020a) revealed drier conditions during 4.3–3.9 ka, continuing the decreasing rainfall trend from ∼5.5 ka (Fig. 6). The drought may have triggered desertification in Inner Mongolia and fed the Hunshandake Sandy Lands (Yang et al., 2015). During this period, dry conditions were also observed in central and western Asia (Carolin et al., 2019; Tan et al., 2021).

This dipole rainfall pattern in monsoonal China inferred from proxy records has been discussed earlier (Tan et al., 2018a; Zhang et al., 2018), but previous studies have drawn this conclusion based on limited records with large dating uncertainties and low resolutions. Here, our multiproxy records provide direct and robust evidence to confirm wet conditions in south-central China during the 4.2 ka event and also support the idea that the 4.2 ka event was not a synchronous global drought event (Railsback et al., 2018; Ön et al., 2021). It is worth noting that the 4.2 ka event recorded in RM8-2 proxies was not marked and rapid like that in other paleorecords such as the abrupt shift in KM-A $\delta^{18}O$ (Mawmluh Cave) profile around 4.0 ka that was used to define the Meghalayan Age (Berkelhammer et al., 2012). The absence of abrupt climatic change during the 4.2 ka event is also evident in the stalagmite records from Oman (Fleitmann et al., 2003) and the western Chinese Loess Plateau (Tan et al., 2020a), which revealed a gradual climatic change during the 4.2 ka event. Ön et al. (2021) reanalyzed 14 paleoclimatic records from southeastern Europe and southwestern Asia that claimed to find abrupt climatic change during the 4.2 ka event and demonstrated that not all records show an abrupt drying anomaly. Some drying shifts lasted for several centuries, and some changes were insignificant (Ön et al., 2021). Moreover, some regional records even found no compelling evidence of the 4.2 ka event; for example, in the northern North Atlantic (Bradley and Bakke, 2019) and Rodrigues Island (Li et al., 2018). The relatively inconspicuous feature of the 4.2 ka event in RM8-2 proxies is also evident in the reconstructed regional precipitation between HS and DG Caves (Hu et al., 2008) and SN $\delta^{13}C$ sequence (Zhang et al., 2021; Fig. 6), suggesting it may be a common climatic signal in south-central China.

The dipole climatic pattern in China during the 4.2 ka event was likely induced by the weakened EASM and the counterbalance between the EASM and westerlies (Tan et al., 2018a). As the paleo-dust record in Japan Sea revealed, the westerlies shifted to a relatively northern position during 5.6–4.3 ka (Nagashima et al., 2013). The decreased EASM intensity that was modulated by the Northern Hemisphere summer insolation dominated the declining rainfall trend in both northern and southern China during this period (Wang et al., 2005; Zhang et al., 2019; Tan et al., 2020a). Afterward, EASM intensity weakened further (Wang et al., 2005), but the westerlies shifted southward and strengthened somewhat due to the weakened Atlantic Meridional Overturning Circulation (Broecker, 1994; Mayewski et al., 1997; Nagashima et al., 2013). These changes caused the migration of the moisture-carrying summer monsoon to the south and resulted in the contrasting conditions in the south (wet) and north (dry) of China (Tan et al., 2018a).

Superimposed on the overall increasing precipitation during 4.3–3.9 ka, there are several multidecadal-scale pulses of wet conditions recorded in the rainfall index and Sr/Ca of RM8-2 and in the reconstructed regional precipitation (Hu et al., 2008) and SN $\delta^{13}C$ profile (Zhang et al., 2021; Fig. 6). The two most remarkable pluvial pulses in our records occurred at 4.25–4.12 and 4.0–3.9 ka (Fig. 6). These observations are consistent with the magnetic-based peatland (Dajiuhu) and speleothem (HS Cave) records from the middle Yangtze River (Xie et al., 2013; Zhu et al., 2017). Additionally, paleohydrological investigations have identified unambiguous paleoflood sediments at archaeological sites (Chengdu Plain, Jinsha, Zhongqiao, Maqiao, Taihu basin) around the upper, middle, and lower reaches of the Yangtze River (Yu et al., 2000; Zhang et al., 2005; Zeng et al., 2016; Jia et al., 2017; Wu et al., 2017; Fig. 1), which likely coincide with the pluvial pulses inferred from our records within the margin of age errors.

Moreover, a large body of evidence suggests that floods also swept across the Yellow River region during this period. For

https://doi.org/10.1017/qua.2022.11 Published online by Cambridge University Press

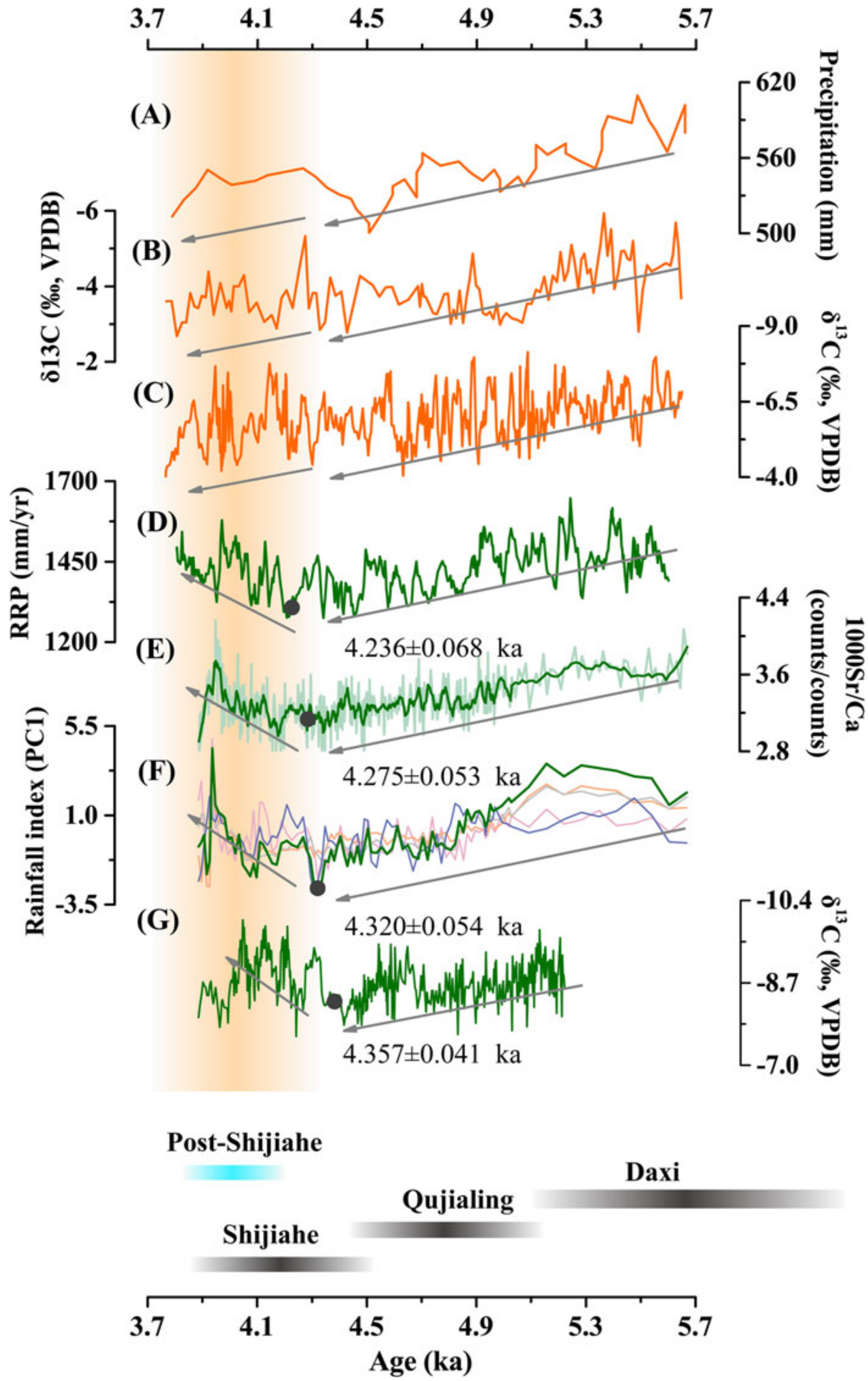

Figure 6. Comparison of stalagmite records from Remi (RM) Cave with other paleohydroclimatic records. (A) Pollen-reconstructed rainfall from Gonghai (GH) Lake (Chen et al., 2015). (B) Speleothem $\delta^{13}C$ record from Liuli (LL) Cave (Zhao et al., 2021). (C) Speleothem $\delta^{13}C$ record from Wuya (WY) Cave (Tan et al., 2020). (D) Reconstructed regional precipitation (RRP), which is obtained by differencing coeval $\delta^{18}O$ values of Heshang (HS) and Dongge (DG) Caves (Hu et al., 2008). (E) X-ray fluorescence (XRF)-scanned Sr/Ca records of RM8-2 (light green) and 10 year smoothed record (green, this study). (F) PC1 (green) of RM8-2 $\delta^{13}C$ (purple), Mg/Ca (pink), Sr/Ca (orange), and Ba/Ca (gray) records as regional rainfall index. (G) Speleothem $\delta^{13}C$ record from Shennong (SN) Cave (Zhang et al., 2021). The gray arrows denote the trends of the sequences before and after ~4.3 ka. The trends are in opposite directions in D–G. The specific change points and 1σ error, which are measured by a parametric nonlinear regression technique (Mudelsee, 2009), are marked by the black dots and numbers in D–G. In addition, the vertical orange bar marks the 4.2 ka event. During the study period, the Daxi, Qujialing, and Shijiahe cultures flourished in the Hanjiang Plain region (horizontal black bar).

example, a highly resolved and accurately dated stalagmite study from WY Cave revealed two megafloods at ~4.2 ka and ~4.0 ka in the middle-lower Yellow River region (Tan et al., 2018b), consistent with paleoflood slackwater deposits in the branches (Damajia, Qishuihe, Jinghe, Weihe, Beiluohe, and Yihe Rivers) of the Yellow River (Huang et al., 2010, 2011, 2012; Ma et al., 2014; Shen et al., 2015; Y. Zhang et al., 2013, 2015) and archaeological sites in Henan Province (Zhang and Xia, 2011; Fig. 1). The

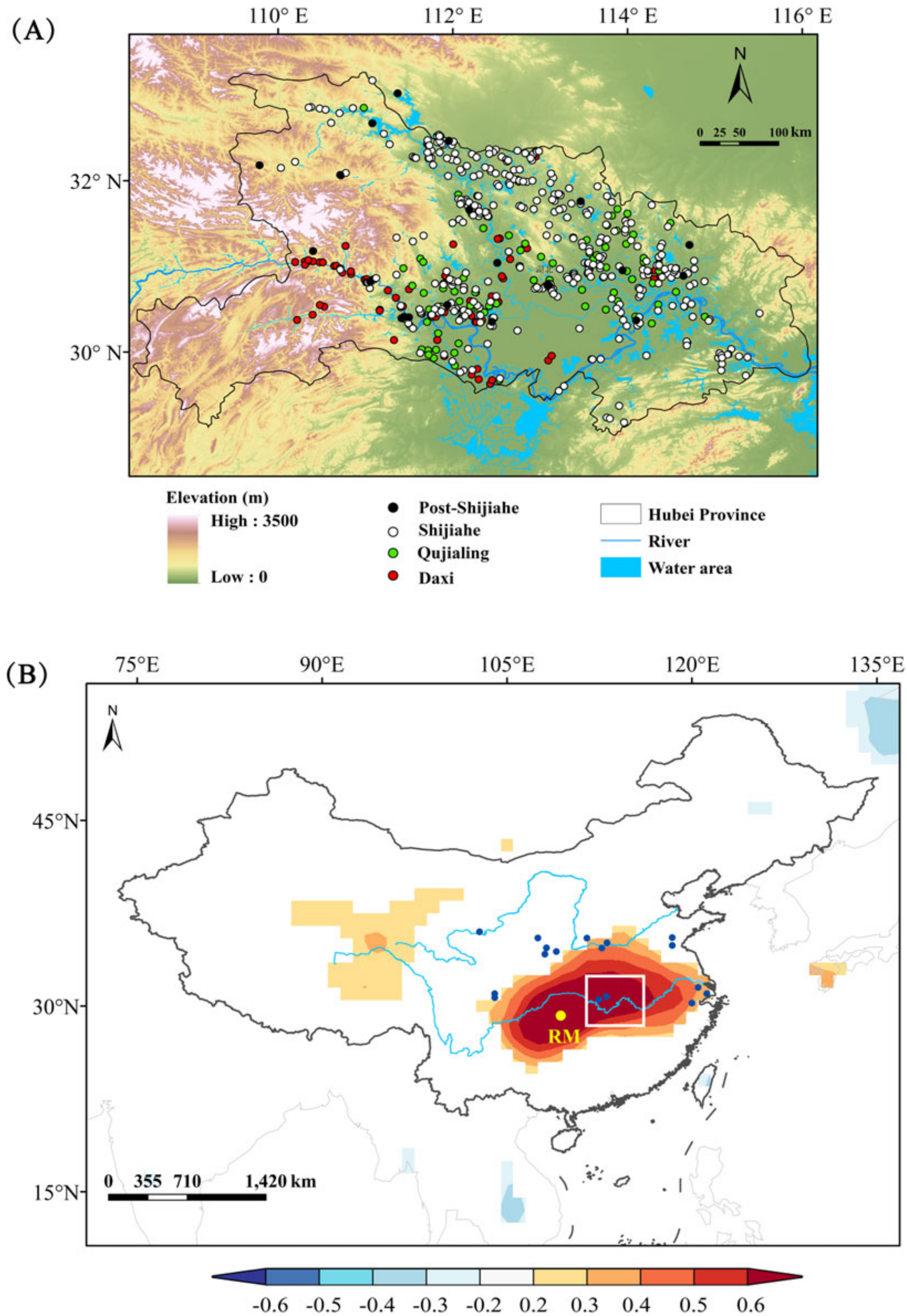

Figure 7. (A) The settlement sites in Hubei Province during Neolithic times, including Daxi, Qujialing, Shijiahe, and post-Shijiahe cultures. The distribution of the sites during the post-Shijiahe culture was revised from Zhong (2019). The information for the sites during other cultural periods can be seen in the State Administration of Cultural Heritage of China (2002) and Xie et al. (2013). The digital elevation model (DEM) of the region is also displayed in A, with the data downloaded from Geospatial Data Cloud: http://www.gscloud.cn. (B) The spatial correlation between annual precipitation around Remi (RM) Cave (yellow dot) and the averaged CRU TS4.0 precipitation anomaly (detrend) during 1951–2019 CE (download from https://www.ncdc.noaa.gov). The scale on the bottom shows the correlation coefficients represented by different colors. The small deep-blue dots mark the records of catastrophic floods during the 4.2 ka event. The white box in B marks the region of A.

evidence confirms the legend of the Great Flood and the Xia dynasty to some extent (Tan et al., 2018b). This also indicates that extreme climate events are independent of general climatic conditions. Heavy rainfalls could also occur in a dry climate setting.

The 4.2 ka event and the collapse of Shijiahe culture

Paleobotanical evidence for rice was found in the middle reaches of the Yangtze River as early as the Pengtoushan culture period (9.0–8.0 ka) (Zhang, 1996), which evolved into rice-dominated agricultural settlements around Jianghan Plain in Hubei Province (State Administration of Cultural Heritage of China, 2002). During the study period, Hubei Province was home to the Daxi (6.3–5.1 ka), Qujialing (5.1–4.5 ka), and Shijiahe cultures (4.5 ka to 4.1–3.9 ka) in succession (Fig. 7A). The development and settlement of these cultures are described in detail by the State Administration of Culture Heritage of China (2002). The projection of the settlement sites onto a modern digital elevation model (DEM) shows that Daxi sites were situated in higher-elevation lands in western Hubei (Fig. 7A). Post-Daxi culture, the Qujialing sites migrated basinward/eastward, where rivers and lakes are located, and the Shijiahe sites expanded further toward the north and south relative to the Qujialing culture (Fig. 7A). Meanwhile, the number of the sites of these two cultures increased. Previous studies suggested that these variations were primarily controlled by the hydroclimatic changes in the region (Zhu et al., 2007; Xie et al., 2013). There is a significant correlation in annual precipitation between Hubei Province and the area around the RM Cave. Therefore, our rainfall reconstruction from the RM Cave potentially provides the rainfall history of Hubei (Fig. 7B). Our data show a long-term trend to drier conditions during 5.6–4.3 ka. The shift of the settlements to the riparian zone seems to correspond with the gradual decreasing rainfall trend during this time, as the rivers and lakes in the floodplain in central and eastern Hubei may have shrunk (Zhu et al., 2007). More land surfaces in the floodplain were exposed and became suitable for habitat (Zhu et al., 2007). This is supported by the trend of deceasing sea level during this time, inferred from the total sulfur content results from Tougou-ike Lake in Japan (Kato et al., 2003). Hence, people moved to the lower lands for water. With the aid of DEM, Xie et al. (2013) estimated that more than 47% of the Qujiangling and Shijiahe sites were situated in lowlands, 15% higher than the sites of the Chengbeixi culture (7.8–6.9 ka, an early Neolithic culture) when regional conditions were wet. These cultures flourished in the hilly lowlands during 5.8–4.3 ka. For example, archaeological excavations suggest that Qujialing culture was characterized by developed farming, sophisticated artifacts, and unique courtyard buildings (State Administration of Cultural Heritage of China, 2002). This was a milestone for prehistoric Chinese civilization, and its impacts expanded to central and southern Henan, southeastern Shaanxi Province, and northern Shanxi Province (Meng, 2011). The Shijiahe culture, which succeeded the Qujialing culture, is thought to have developed a state-like civilization system (Han, 2016). Yasuda et al. (2004) suggested that the aridification of the climate resulted in a population explosion in the river valleys and the appearance of urban civilization in the region. This is in contrast with the view that the drought climate, which was unfavorable for rice cultivation, triggered the collapse of Shijiahe culture in the Late Neolithic period (Liu and Feng, 2012).

We suggest that unlike northern China, where drought conditions pushed cultures such as the Xiaoheyan (5.0–4.2/4.0 ka) and Longshan cultures (4.5–4.0 ka) (Cai et al., 2021; Zhao et al., 2021), into recession in the late mid-Holocene stage, decreasing precipitation in south-central China was in general beneficial for cultural development. This mechanism has been used to explain the unprecedented prosperity of the Baodun culture (Zeng et al., 2016; Jia et al., 2017) and the well-known Liangzhu culture (Zhang et al., 2005; Zhang et al., 2021) in the lowlands of the upper and lower reaches of the Yangtze River in the 5.0-4.3 ka dry period.

After 4.3 ka, the regional climate transitioned gradually to wetter conditions, as evidenced by our speleothem data, which is consistent with the expansion of Yunmengze Lake in the floodplain (Zhou, 1994) and the increasing sea level in Japan (Kato et al., 2003). This may have threatened the majority of Shijiahe sites in low-lying lands. The floods during the 4.2 ka event may have also impeded the development of Shijiahe culture, although archaeological data show that water management systems to prevent floods appeared in some Qujialing and Shijiahe sites (e.g., Taojiahu, Xiaocheng, Menbanwan) (Liu, 2021). As a result, the Shijiahe sites were greatly reduced and subsequent sites were located on higher-elevation land during 4.1–3.9 ka (Fig. 7A). In addition, a growing number of archaeological studies found the characteristics of artifacts (e.g., pottery, jade ware) changed drastically during this time compared with the early to middle Shijiahe stage, integrating new features from Wangwan III culture from the central plain (Han and Yang, 1997; He, 2006). Hence, some archaeologists defined this culture system to be post-Shijiahe culture (Meng, 1997) or named it after the archaeological sites, such as Sanfangwan culture (Wang, 2007) and Xiaojiawuji culture (He, 2006). This implies cultural exchanges occurred in the region during the Late Neolithic period, which are thought to be related to the Yu's Battle against Sanmiao Ethnic Groups (Han, 2020a, 2020b). Indeed, many archaeologists and historians have suggested the people of the Shijiahe culture were probably the Sanmiao tribe, and people of the Wangwan III culture were the Yu tribe (Han, 2020a, 2020b and references therein). It is plausible that Yu took advantage of the climate transition to expand southward and defeat the Sanmiao tribe, accelerating the fall of the Shijiahe culture (Li et al., 2013; Jia et al., 2017).

Similar climate deterioration was also identified in the upper and lower reaches of the Yangtze River during the 4.2 ka event, but their effects were different. Similar to the variations seen at Shijiahe sites, the archaeology and paleoclimatic studies in the Chengdu Plain indicate that Baodun settlements were forced to migrate from low-lying areas to higher elevations due to frequent floods (Zeng et al., 2016; Jia et al., 2017). However, Liangzhu settlements, which were based in the Yangtze delta, had no buffer to protect them from floods. Catastrophic paleofloods or rising sea levels have been widely and directly connected to the demise of Liangzhu culture by archaeologists (Zhang et al., 2005; Zhang et al., 2021). This implies that topographic features play an important role in cultural development.

CONCLUSIONS

Our study suggests that south-central China experienced a gradual dry-to-wet transition at ∼4.3 ka, which is consistent with other records from southern and central China but in contrast to climatic conditions in northern China. However, both northern and southern China experienced several intense pluvial periods

https://doi.org/10.1017/qua.2022.11 Published online by Cambridge University Press

during the 4.2 ka event, leading to more than two megafloods in the Yellow River and Yangtze River regions. Taking into account the archaeological evidence and the DEM, we suggest that the development of rice-cultivating prehistoric cultures (Daxi, Qujialing, and Shijiahe cultures in succession) in Jianghan Plain was highly dependent on regional hydroclimatic conditions during the low-productivity stage, as well as regional topographic features. The settlement sites expanded in the river valley in the dry climate period of 5.6–4.3 ka. However, they were damaged afterward by enhanced rainfall and frequent floods. At the same time, the Wangwan III culture from the central plain attacked them, leading to the final collapse of the Shijiahe culture.

Financial Support. This research was supported by the Strategic Priority Research Program of Chinese Academy of Sciences (XDB40000000), the National Key Research and Development Program of China (2017YFA0603401), and the PIFI Program of Chinese Academy of Sciences (2020VCA0019). The dating work was partially supported by the U.S. National Science Foundation (1702816 to R.L.E.).

REFERENCES

Berkelhammer, M., Sinha, A., Stott, L., Cheng, H., Pausata, F.S.R., Yoshimura, K., 2012. An abrupt shift in the Indian monsoon 4000 years ago. *Geophysical Monograph Series* **198**, 75–88.

Bond, G., Showers, W., Cheseby, M., Lotti, R., Almasi, P., deMenocal, P., Priore, P., Cullen, H., Hajdas, I., Bonani, G., 1997. A pervasive millennial-scale cycle in North Atlantic Holocene and glacial climates. *Science* **278**, 1257–1266.

Bradley, R.S., Bakke, J., 2019. Is there evidence for a 4.2 ka BP event in the northern North Atlantic region? *Climate of the Past* **15**, 1665–1676.

Breitenbach, S.F.M., Rehfeld, K., Goswami, B., Baldini, J.U.L., Ridley, H.E., Kennett, D.J., Prufer, K.M., *et al.*, 2012. Constructing proxy records from age models (COPRA). *Climate of the Past* **8**, 1765–1779.

Broecker, W.S., 1994. Massive iceberg discharges as triggers for global climate change. *Nature* **372**, 421–424.

Cai, Y., Cheng, X., Ma, L., Mao, R., Breitenbach, S.F.M., Zhang, H., Xue, G., Cheng, H., Edwards, R.L., An, Z., 2021. Holocene variability of East Asian summer monsoon as viewed from the speleothem δ^{18}O records in central China. *Earth and Planetary Science Letters* **558**, 116758.

Carolin, S.A., Walker, R.T., Day, C.C., Ersek, V., Sloan, R.A., Dee, M.W., Talebian, M., Henderson, G.M., 2019. Precise timing of abrupt increase in dust activity in the Middle East coincident with 4.2 ka social change. *Proceeding of the National Academy of Science USA* **116**, 67–72.

Chen, F., Xu, Q., Chen, J., Birks, H.J.B., Liu, J., Zhang, S., Jin, L., *et al.*, 2015. East Asian summer monsoon precipitation variability since the last deglaciation. *Scientific Reports* **5**, 11186.

Cheng, H., Edwards, R.L., Shen, C., Polyak, V.J., Asmerom, Y., Woodhead, J., Hellstrom, J., *et al.*, 2013. Improvements in ^{230}Th dating, ^{230}Th and ^{234}U half-life values, and U-Th isotopic measurements by multi-collector inductively coupled plasma mass spectrometry. *Earth and Planetary Science Letters* 371–372, 82–91.

Cheng, H., Edwards, R.L., Sinha, A., Spötl, C., Yi, L., Chen, S., Kelly, M., *et al.*, 2016a. The Asian monsoon over the past 640,000 years and ice age terminations. *Nature* **534**, 640–646.

Cheng, H., Spötl, C., Breitenbach, S.F.M., Sinha, A., Wassenburg, J.A., Jochum, K.P., Scholz, D., *et al.*, 2016b. Climate variations of Central Asia on orbital to millennial timescales. *Scientific Reports* **6**, 36975.

Cheng, H., Zhang, H., Zhao, J., Li, H., Ning, Y., Kathayat, G., 2019. Chinese stalagmite paleoclimate researches: a review and perspective. *Science China-Earth Sciences* **62**, 1489–1513.

Cosford, J., Qing, H., Eglington, B., Mattey, D., Yuan, D., Zhang, M., Cheng, H., 2008. East Asian monsoon variability since the mid-Holocene recorded in a high-resolution, absolute-dated aragonite speleothem from eastern China. *Earth and Planetary Science Letters* **275**, 296–307.

Cosford, J., Qing, H., Mattey, D., Eglington, B., Zhang, M., 2009. Climatic and local effects on stalagmite δ^{13}C values at Lianhua Cave, China. *Palaeogeography Palaeoclimatology Palaeoecology* **280**, 235–244.

deMenocal, P.B., 2001. Cultural responses to climate change during the late Holocene. *Science* **292**, 667–673.

Dong, G., Li, T., Zhang, S., Ren, L., Li, R., Li, G., Xiao, Y., Wang, Z., Chen, F., 2021. Precipitation in surrounding mountains instead of lowlands facilitated the prosperity of ancient civilizations in the eastern Qaidam Basin of the Tibetan Plateau. *Catena* **203**, 105318.

Dong, J., Wang, Y., Cheng, H., Hardt, B., Edwards, R. L., Kong, X., Wu, J., *et al.*, 2010. A high-resolution stalagmite record of the Holocene East Asian monsoon Mt Shennongjia, central China. *The Holocene* **20**, 257–264.

Dorale, J.A., Liu, Z., 2009. Limitations of Hendy Test criteria in judging the paleoclimatic suitability of speleothems and the need for replication. *Journal of Cave and Karst Studies* **71**, 73–80.

Dykoski, C.A., Edwards, R.L., Cheng, H., Yuan, D., Cai, Y., Zhang, M., Lin, Y., Qing, J., An, Z., Revenaugh, J., 2005. A high-resolution, absolute-dated Holocene and deglacial Asian monsoon record from Dongge Cave, China. *Earth and Planetary Science Letters* **233**, 71–86.

Edwards, R.L., Chen, J.H., Wasserburg, G.J., 1987. ^{238}U-^{234}U-^{230}Th-^{232}Th systematics and the precise measurement of time over the past 500,000 years. *Earth and Planetary Science Letters* **81**, 175–192.

Fairchild, I.J., Borsato, A., Tooth, A.F., Frisia, S., Hawkesworth, C.J., Huang, Y., McDermott, F., Spiro, B., 2000. Controls on trace element (Sr-Mg) compositions of carbonate cave waters: implications for speleothem climatic records. *Chemical Geology* **166**, 255–269.

Fairchild, I.J., Treble, P.C., 2009. Trace elements in speleothems as recorders of environmental change. *Quaternary Science Reviews* **28**, 449–468.

Fleitmann, D., Burns, S.J., Mudelsee, M., Neff, U., Kramers, J., Mangini, A., Matter, A., 2003. Holocene forcing of the Indian monsoon recorded in a stalagmite from southern Oman. *Science* **300**, 1737–1739.

Fohlmeister, J., Scholz, D., Kromer, B., Mangini, A., 2011. Modelling carbon isotopes of carbonates in cave drip water. *Geochimica et Cosmochimica Acta* **75**, 5219–5228.

Genty, D., Baker, A., Massault, M., Proctor, C., Gilmour, M., Pons-Branchu, E., Hamelin, B., 2001. Dead carbon in stalagmites: carbonate bedrock paleodissolution vs. ageing of soil organic matter. Implications for ^{13}C variations in speleothems. *Geochimica et Cosmochimica Acta* **65**, 3443–3457.

Genty, D., Blamart, D., Ouahdi, R., Gilmour M., Baker, A., Jouzel, J., Van-Exter, S., 2003. Precise dating of Dansgaard-Oeschger climate oscillations in western Europe from stalagmite data. *Nature* **421**, 833–837.

Han, J., 2016. A comparison of civilized course between the central plain and Jianghan area. [In Chinese with English abstract.] *Jianghan Archaeology* **6**, 39–44

Han, J., 2020a. Neolithic wars and the course of the early Chinese civilization. [In Chinese with English abstract.] *Social Science Front: Military and Political History* **10**, 99–107.

Han, J., 2020b. Violent cultural changes in Longshan period and tribal warfare in Chinese legendary era. [In Chinese with English abstract.] *Social Sciences* **1**, 152–163.

Han, J., Yang X., 1997. A study of the Wangwan III culture. [In Chinese with English abstract.] *Acta Archaeolofica Sinica* **1**, 1–22.

He, N., 2006. The discussion on the Xiaojiawuji culture and its related issues. [In Chinese.] *Archaeology of the Three Dynasties* (*Two*), 98–145

Hu, C., Henderson, G.M., Huang, J., Xie, S., Sun, Y., Johnson, K.R., 2008. Quantification of Holocene Asian monsoon rainfall from spatially separated cave records. *Earth and Planetary Science Letters* **266**, 221–232.

Huang, C., Pang, J., Zha, X., Su, H., Jia, Y., 2011. Extraordinary floods related to the climatic event at 4200 a BP on the Qishuihe River, middle reaches of the Yellow River, China. *Quaternary Science Reviews* **30**, 460–468.

Huang, C., Pang, J., Zha, X., Zhou, Y., Su, H., Li, Y., 2010. Extraordinary floods of 4100-4000 a BP recorded at the Late Neolithic ruins in the Jinghe River gorges, middle reach of the Yellow River, China. *Palaeogeography Palaeoclimatology Palaeoecology* **289**, 1–9.

Huang, C., Pang, J., Zha, X., Zhou, Y., Su, H., Zhang, Y., Wang, H., Gu, H., 2012. Holocene palaeoflood events recorded by slackwater deposits along the lower Jinghe River valley, middle Yellow River basin, China. *Journal of Quaternary Science* **27**, 485–493.

Huang, X., Lin, D., Wang, J., Chang, S., 2013. Temporal and spatial NPP variation in the karst region in South China under the background of climate change. [In Chinese with English abstract.] *Scientia Silvae Sinicae* **49**, 10–16.

Huang, Y.M., Fairchild, I.J., Borsato, A., Frisia, S., Cassidy, N.J., McDermott, F., Hawkesworth, C.J., 2001. Seasonal variations in Sr, Mg and P in modern speleothems (Grotta di Ernesto, Italy). *Chemical Geology* **175**, 429–448.

Jia, T., Ma, C., Zhu, C., Guo, T., Xu, J., Guan, H., Zeng, M., Huang, M., Zhang, Q., 2017. Depositional evidence of palaeofloods during 4.0-3.6 ka BP at the Jinsha site, Chengdu Plain, China. *Quaternary International* **440**, 78–89.

Kato, M., Fukusawa, H., Yasuda, Y., 2003. Varved lacustrine sediments of Lake Tougou-ike, western Japan, with reference to Holocene sea-level changes in Japan. *Quaternary International* **105**, 33–37.

Li, B., Zhu, C., Wu, L., Li, F., Sun, W., Wang, X., Liu, H., Meng, H., Wu, D., 2013. Relationship between environmental change and human activities in the period of the Shijiahe culture, Tanjialing site, Jianghan Plain, China. *Quaternary International* 308–309, 45–52.

Li, D., Tan, L., Cai, Y., Jiang, X., Ma, L., Cheng, H., Edwards, R.L., Zhang, H., Gao, Y., An, Z., 2019a. Is Chinese stalagmite δ^{18}O solely controlled by the Indian summer monsoon? *Climate Dynamic* **53**, 2969–2983.

Li, D., Tan, L., Guo, F., Cai, Y., Sun, Y., Xue, G., Cheng, X., *et al.*, 2019b. Application of Avaatech X-ray fluorescence core-scanning in Sr/Ca analysis of speleothems. *Science China-Earth Sciences* **62**, 964–973.

Li, H., Cheng, H., Sinha, A., Kathayat, G., Spötl, C., André, A.A., Meunier, A., *et al.*, 2018. Hydro-climatic variability in the southwestern Indian Ocean between 6000 and 3000 years ago. *Climate of the Past* **14**, 1881–1891.

Liu, F., Feng, Z., 2012. A dramatic climatic transition at ∼4000 cal. yr BP and its cultural responses in Chinese cultural domains. *The Holocene* **22**, 1181–1197.

Liu, J., 2021. Preliminary exploration of prehistoric water control civilization in China. [In Chinese with English abstract.] *Cultural Relics in Southern China* **6**, 5–11.

Liu, Z., Qu, Y., 2019. Vegetation change and its response to climate change based on SPOT-VGT in Hunan Province of southern China. [In Chinese with English abstract.] *Journal of Beijing Forestry University* **41**, 80–87.

Maher, B.A., Thompson, R., 2012. Oxygen isotopes from Chinese caves: records not of monsoon rainfall but of circulation regime. *Journal of Quaternary Science* **27**, 615–624.

Ma, M., Dong, G., Chen, F., Meng, X., Wang, Z., Elston, R., Li, G., 2014. Process of paleofloods in Guanting basin, Qinghai Province, China and possible relation to monsoon strength during the mid-Holocene. *Quaternary International* **321**, 88–96.

Mayewski, P.A., Meeker, L.D., Twickler, M.S., Whitlow, S., Yang, Q., Lyons, W.B., Prentice, M., 1997. Major features and forcing of high-latitude northern hemisphere atmospheric circulation using a 110,000-year-long glaciochemical series. *Journal of Geophysical Research Oceans* **102**, 26345–26366.

McDermott, F., 2004. Palaeo-climate reconstruction from stable isotope variations in speleothems: a review. *Quaternary Science Reviews* **23**, 901–918.

Meng, H., 1997. *Prehistoric Culture Structure in the Middle Reaches of the Yangtze River*. [In Chinese.] Yangtze Literature and Art Press, Wuhan.

Meng, Y., 2011. The northward spread of Qujialing culture. [In Chinese with English abstract.] *Huaxia Archaeology* **3**, 51–63.

Mudelsee, M., 2009. Break function regression: a tool for quantifying trend changes in climate time series. *European Physical Journal-Special Topics* **174**, 49–63.

Nagashima, K., Tada, R., Toyoda, S., 2013. Westerly jet-East Asian summer monsoon connection during the Holocene. *Geochemistry Geophysics Geosystems* **14**, 5041–5053.

Novello, V.F., Cruz, F.W., McGlue, M.M., Wong, C.I., Ward, B.M., Vuille, M., Santos, R.A., *et al.*, 2019. Vegetation and environmental changes in tropical South America from the last glacial to the Holocene documented by multiple cave sediment proxies. *Earth and Planetary Science Letters* **524**, 115717.

Ön, Z.B., Greaves, A.M., Akcer-Ön, S., Özeren, M.S., 2021. A Bayesian test for the 4.2 ka BP abrupt climatic change event in southeast Europe and southwest Asia using structural time series analysis of paleoclimate data. *Climatic Change* **165**, 7.

Railsback, L.B., Liang, F., Brook, G.A., Voarintsoa, N.R.G., Sletten, H.R., Marais, E., Hardt, B., Cheng, H., Edwards, R.L., 2018. The timing, two-pulsed nature, and variable climatic expression of the 4.2 ka event: a review and new high-resolution stalagmite data from Namibia. *Quaternary Science Reviews* **186**, 78–90.

Ronay, E.R., Breitenbach, S.F.M., Oster, J.L., 2019. Sensitivity of speleothem records in the Indian Summer Monsoon region to dry season infiltration. *Scientific Reports* **9**, 5091.

Shen, H., Yu, L., Zhang, H., Zhao, M., Lai, Z., 2015. OSL and radiocarbon dating of flood deposits and its paleoclimatic and archaeological implications in the Yihe River Basin, East China. *Quaternary Geochronology* **30**, 398–404.

Sinha, A., Kathayat, G., Weiss, H., Li, H., Cheng, H., Reuter, J., Schneider, A.W., *et al.*, 2019. Role of climate in the rise and fall of the Neo-Assyrian Empire. *Science Advances* **5**, eaax6656.

State Administration of Cultural Heritage of China, 2002. *Cultural Relics Atlas of China. Part 1, Hubei Province*. [In Chinese.] Map Press of Xi'an, Xi'an, China.

Staubwasser, M., Sirocko, F., Grootes, P.M., Segl, M., 2003. Climate change at the 4.2 ka BP termination of the Indus valley civilization and Holocene south Asian monsoon variability. *Geophysical Research Letters* **30**, 1425.

Sun, Q., Liu, Y., Wünnemann, B., Peng, Y., Jiang, X., Deng, L., Chen, J., Li, M., Chen, Z., 2019. Climate as a factor for Neolithic cultural collapses approximately 4000 years BP in China. *Earth-Science Reviews* **197**, 102915.

Tan, L., Cai, Y., Cheng, H., Edwards, R.L., Gao, Y., Xu, H., Zhang, H., An, Z., 2018a. Centennial- to decadal-scale monsoon precipitation variations in the upper Hanjiang River region, China over the past 6650 years. *Earth and Planetary Science Letters* **482**, 580–590.

Tan, L., Dong, G., An, Z., Edwards, R.L., Li, H., Li, D., Spengler, R., *et al.*, 2021. Megadrought and cultural exchange along the proto-silk road. *Science Bulletin* **66**, 603–611.

Tan, L., Liu, W., Wang, T., Cheng, P., Zang, J., Wang, X., Ma, L., *et al.*, 2020b. A multiple-proxy stalagmite record reveals historical deforestation in central Shandong, northern China. *Science China-Earth Sciences* **63**, 1622–1632.

Tan, L., Li, Y., Wang, X., Cai, Y., Lin, F., Cheng, H., Ma, L., Sinha, A., Edwards, R.L., 2020a. Holocene monsoon change and abrupt events on the western Chinese Loess Plateau as revealed by accurately dated stalagmites. *Geophysical Research Letters* **46**, e2020GL090273.

Tan, L., Shen, C., Cai, Y., Cheng, H., Edwards, R.L., 2018b. Great flood in the middle-lower Yellow River reaches at 4000 a BP inferred from accurately-dated stalagmite records. *Science Bulletin* **63**, 206–208.

Tan, L., Shen, C., Cai, Y., Lo, L., Cheng, H., An, Z., 2014. Trace-element variations in an annually layered stalagmite as recorders of climatic changes and anthropogenic pollution in Central China. *Quaternary Research* **81**, 181–188.

Treble, P., Shelley, J.M.G., Chappell, J., 2003. Comparison of high resolution sub-annual records of trace elements in a modern (1911-1992) speleothem with instrumental climate data from southwest Australia. *Earth and Planetary Science Letters* **216**, 141–153.

Wang, C., Bendle, J.A., Zhang, H., Yang, Y., Liu, D., Huang, J., Cui, J., Xie, S., 2018. Holocene temperature and hydrological changes reconstructed by bacterial 3-hydroxy fatty acids in a stalagmite from central China. *Quaternary Science Reviews* **192**, 97–105.

Wang, H., 2013. Viewing the decline of Sanmiao culture from the archaeological remains in the heartland of Shijiahe culture. [In Chinese.] *Jintian: Historical Philosophy* **300**, 120–121

Wang, J., 2007. On Post-Shijihe culture: terminology. *Jianghan Archaeology* 102, 60–72.

Wang, W., 2013. *The Karst Features Research and Potential Calculation on Carbon Sink in the Basin of Dalongdong Underground in the Hunan Province*. [In Chinese with English abstract.] Master's thesis, Guangxi Teachers Education University, Guilin Guangxi Province, China.

Wang, Y., Cheng, H., Edwards, R.L., He, Y., Kong, X., An, Z., Wu, J., Kelly, M.J., Dykoski, C.A., Li, X., 2005. The Holocene Asian monsoon: links to solar changes and North Atlantic climate. *Science* **308**, 854–857.

Wassenburg, J.A., Scholz, D., Jochum, K.P., Cheng, H., Oster, J., Immenhauser, A., Richter, D.K., *et al.*, 2016. Determination of aragonite trace element distribution coefficients from speleothem calcite–aragonite transitions. *Geochimica et Cosmochimica Acta* **190**, 347–367.

Watanabe, T.K., Watanabe, T., Yamazaki, A., Pfeiffer, M., 2019. Oman corals suggest that a stronger winter shamal season caused the Akkadian Empire (Mesopotamia) collapse. *Geology* **47**, 1141–1145.

Weiss, H., Bradley, R.S., 2001. What drives societal collapse? *Science* **291**, 609–610.

Weiss, H., Courty, M.A., Wetterstrom, W., Guichard, F., Senior, L., Meadow, R., Curnow, A., 1993. The genesis and collapse of third millennium North Mesopotamian civilization. *Science* **261**, 995–1004.

Wu, L., Zhu, C., Ma, C., Li, F., Meng, H., Liu, H., Li, L., Wang, X., Sun, W., Song, Y., 2017. Mid-Holocene palaeoflood events recorded at the Zhongqiao Neolithic cultural site in the Jianghan Plain, middle Yangtze River Valley, China. *Quaternary Science Reviews* **173**, 145–160.

Wu, W., Liu, T., 2004. Possible role of the "Holocene Event 3" on the collapse of Neolithic cultures around the Central Plain of China. *Quaternary International* **117**, 153–166.

Xiao, J., Zhang, S., Fan, J., Wen, R., Zhai, D., Tian, Z., Jiang, D., 2018. The 4.2 ka event: multi-proxy records from a closed lake in the northern margin of the East Asian summer monsoon. *Climate of the Past* **14**, 1417–1425.

Xie, S., Evershed, R.P., Huang, X., Zhu, Z., Pancost, R.D., Meyers, P.A., Gong, L., *et al.*, 2013. Concordant monsoon-driven postglacial hydrological changes in peat and stalagmite records and their impacts on prehistoric cultures in central China. *Geology* **41**, 827–830.

Xue, G., Cai, Y., Lu, Y., Ma, L., Cheng, X., Liu, C., Yan, H., *et al.*, 2021. Speleothem-based hydroclimate reconstructions during the penultimate deglaciation in Northern China. *Paleoceanography and Paleoclimatology* **36**, e2020PA004072.

Yang, X., Scuderi, L.A., Wang, X., Scuderi, L.J., Zhang, D., Li, H., Forman, S., *et al.*, 2015. Groundwater sapping as the cause of irreversible desertification of Hunshandake Sandy Lands, Inner Mongolia, northern China. *Proceeding of the National Academy of Science USA* **112**, 702–706.

Yasuda, Y., Fujiki, T., Nasu, H., Kato, M., Morita, Y., Mori, Y., Kanehara, M., *et al.*, 2004. Environmental archaeology at the Chengtoushan site, Hunan Province, China, and implications for environmental change and the rise and fall of the Yangtze River civilization. *Quaternary International* 123–125, 149–158.

Yuan, D., Cheng, H., Edwards, R.L., Dykoski, C.A., Kelly, M.J., Zhang, M., Qing, J., *et al.*, 2004. Timing, duration, and transitions of the last interglacial Asian monsoon. *Science* **304**, 575–578.

Yu, S., Zhu, C., Song, J., Qu, W., 2000. Role of climate in the rise and fall of Neolithic cultures on the Yangtze Delta. *Boreas* **29**, 157–165.

Zeng, M., Ma, C., Zhu, C., Song, Y., Zhu, T., He, K., Chen, J., Huang, M., Jia, T., Guo, T., 2016. Influence of climate change on the evolution of ancient culture from 4500 to 3700 cal. yr BP in the Chengdu Plain, upper reaches of the Yangtze River, China. *Catena* **147**, 742–754.

Zhang, H., Brahim, Y.A., Li, H., Zhao, J., Kathayat, G., Tian, Y., Baker, J., *et al.*, 2019. The Asian summer monsoon: teleconnections and forcing mechanisms—a review from Chinese speleothem $\delta^{18}O$ records. *Quaternary* **2**, 26.

Zhang, H., Cheng, H., Cai, Y., Spötl, C., Kathayat, G., Sinha, A., Edwards, R.L., Tan, L., 2018. Hydroclimatic variations in southeastern China during the 4.2 ka event reflected by stalagmite records. *Climate of the Past* **14**, 1805–1817.

Zhang, H., Cheng, H., Sinha, A., Spötl, C., Cai, Y., Liu, B., Kathayat, G., *et al.*, 2021. Collapse of the Liangzhu and other cultures in the lower Yangtze region in response to climate change. *Science Advances* **7**, eabi9275.

Zhang, H., Yu, K., Zhao, J., Feng, Y., Lin, Y., Zhou, W., Liu, G., 2013. East Asian Summer Monsoon variations in the past 12.5ka: high-resolution $\delta^{18}O$ record from a precisely dated aragonite stalagmite in central China. *Journal of Asian Earth Sciences* **73**, 162–175.

Zhang, J., Xia, Z., 2011. Deposition evidences of the 4 ka BP flood events in central China plains. [In Chinese with English abstract.] *Acta Geographica Sinica* **66**, 685–697.

Zhang, Q., Zhu, C., Liu, C.L., Jiang, T., 2005. Environmental change and its impacts on human settlement in the Yangtze Delta, P.R. China. *Catena* **60**, 267–277.

Zhang, X., 1996. The origin and development of prehistoric rice-farming in the middle reaches of the Yangtze River. [In Chinese.] *Agricultural History of China* **15**, 18–22.

Zhang, Y., Huang, C.C., Pang, J., Zha, X., Zhou, Y., Gu, H., 2013. Holocene paleofloods related to climatic events in the upper reaches of the Hanjiang River valley, middle Yangtze River basin, China. *Geomorphology* **195**, 1–12.

Zhang, Y., Huang, C.C., Pang, J., Zha, X., Zhou, Y., Wang, X., 2015. Holocene palaeoflood events recorded by slackwater deposits along the middle Beiluohe River valley, middle Yellow River basin, China. *Boreas* **44**, 127–138.

Zhao, J., Tan, L., Yang, Y., Pérez-Mejías, C., Brahim, Y.A., Lan, J., Wang, J., Li, H., Wang, T., Zhang, H., Cheng, H., 2021. New insights towards an integrated understanding of NE Asian monsoon during mid to late Holocene. *Quaternary Science Reviews* **254**, 106793.

Zhong, X., 2019. A review of the research on the Post-Shijiahe culture. [In Chinese with English abstract.] *Journal of Archaeology and Museology* **4**, 24–33

Zhou, F., 1994. Historical evolution of Yunmeng marsh and Jingjiang delta. [In Chinese with English abstract.] *Journal of Lake Sciences* **6**, 22–32.

Zhu, C., Zhong, Y., Zheng, C., Ma, C., Li, L., 2007. Relationship of Archaeological sites distribution and environment from the Paleolithic Age to the Warring States time in Hubei Province. [In Chinese with English abstract.] *Acta Geographica Sinica* **62**, 227–242.

Zhu, Z., Feinberg, J.M., Xie, S., Bourne, M.D., Huang, C., Hu, C., Cheng, H., 2017. Holocene ENSO-related cyclic storms recorded by magnetic minerals in speleothems of central China. *Proceeding of the National Academy of Science USA* **114**, 852–857.

https://doi.org/10.1017/qua.2022.11 Published online by Cambridge University Press